

# Original Research Article: Exploring the Inhibition Potential of Carbamodithionic acid on Fe (111) Surface: A Theoretical Study

Ayuba Abdullahi Muhammad<sup>1</sup>, Nyijime Aondofa Thomas<sup>2</sup>, Safiyya AbubakarMinjibir<sup>1</sup>, Najib Usman Shehu<sup>1</sup>, Fater Iorhuna\*<sup>1</sup>

<sup>1</sup>Research Laboratory, Bayero University, Department of Pure and Industrial Chemistry, Kano, 700241, Nigeria

<sup>2</sup>Research Laboratory, Department of Chemistry, Joseph Saawaun Tarka University, Makurdi, Benue, Nigeria



**Citation** A. A. Muhammad, N. A. Thomas, N. U. Shehu, F. Iorhuna\*. Exploring the Inhibition Potential of Carbamodithionic acid on Fe (111) Surface: A Theoretical Study. *J. Eng. Ind. Res.* 2023, 4(4): 201-210.

<https://doi.org/10.48309/jeires.2023.4.2>



## Article info:

Received: 2023-10-13

Accepted: 2023-12-29

ID: JEIRES-2311-1102

Checked for Plagiarism: Yes

Editor who Approved Publication:

Professor Dr. Mohammad Haghighi

## Keywords:

Corrosion, Carbamodithionic acid, Simulation

## ABSTRACT

One of the most widely utilized and reasonably priced materials in the building and construction industry today is mild steel. However, one unfavorable consequence of the abovementioned materials' destruction has been corrosion. Different types of inhibitors have been used adequately to minimize or control the corrosion rate but failed. Using Materials Studio software, the adsorption of carbamodithionic acid on an iron surface was investigated by molecular dynamic (MD) modeling and quantum chemical calculations to check its inhibition performance. Results from molecular dynamic simulations showed that the molecule CTA efficiently adsorbs on the iron surface at an appropriate geometrical optimization. The results of the molecular dynamic simulation showed that the S4=C1-S3 present in the ring, the heteroatoms (N and S) and the pi-bonds are the active sites of the molecule. The ring, the nitrogen and sulfur heteroatoms, and the double bonded carbon atoms in the molecule are the active sites of the molecules according to the quantum chemical calculation based on the natural atomic charge also the frontier molecular orbital, and the Fukui index values. The efficiency of the hetero atoms in terms of the reactivity of the bonds shared with the carbon atom is also demonstrated by bond length evaluated. The inhibitor's bond angles are planar (tend to be 180° or 0°), and it is anticipated that the compound will display SP<sup>2</sup> hybridization with a significant amount of p-orbital character on the metal. The quantum chemical simulation also showed that, the HOMO and LUMO densities increased significantly which can aid adsorption significantly increased by the thio functional group in the molecule and the pi-bond that is connected to the S4-C1 bond. The molecule has high global softness, EHOMO, and lower energy gap values of 2.454, -5.196, and 4.907eV, respectively. It can be employed in minimizing corrosion of mild steel in corrosion environments due to its adsorption potentials. In addition, at the temperature under consideration, the molecule's adsorption capacity closely matches the binding energy of the molecule.

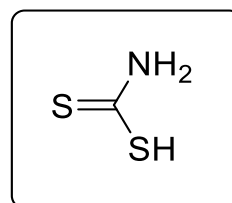
## Introduction

When materials interact with their environment, corrosion-based material deterioration may occur [1-5]. This frequently refers to damage to steel, iron, or metal caused by maintenance on roads, rails, bridges, warehouse cylinders and tanks, utilities and pipes [6]. The possibility of structural collapse increases the moment corrosion is initiated [7]. Corrosion is defined as the natural transformation of a refined metal into a more stable form, such as its oxide, hydroxide, or sulfide state, which causes the substance to deteriorate [8]. The main hazards and effects of corrosion, in addition to its destructive nature of structures, are substantial harm to the body systems such as eyes, skin, respiratory and digestive systems [9]. When it impacts aesthetics, corrosion can reduce a building's or a location's overall value. The environment may be harmed and individuals may be put at danger as a result of blockages in the pipes or mechanical damage to the pumps, valves, etc. [10]. Fluid pollution in pipelines or vessels affects our daily lives in ways that are unrelated to industrial risks, such as when we commute to work or school or while we are out having fun. Corrosion's effects on roads, buildings, electrical towers, and other infrastructure put people in risk and need expensive upkeep. If this collapse due to a section of the metal that is rusted or weak, a disaster might result [11].

According to some studies, the usage of inhibitive compounds that either includes pi or certain heteroatoms N, S, P, and O can help to mitigate the level of corrosion-causing interaction between metals and their surroundings [12]. These compounds are thought to coat the surface of mild steel in layers, increasing the metal's ability to absorb material which in turn increase the metal's adsorption capacity, and lower the rate of corrosion on the metal's surface by blocking the active sites on the particular metal [13].

A number of researchers have investigated the usage of the experimental technique since time

immemorial. Nevertheless, the process is time-consuming and rife with human error. To the best of our knowledge, neither the structure of Carbamodithionic acid (CTA) nor its adsorption potentials has been theoretically studied using Fe as a reference metal. Hence, in this study since mild steel is one of the most often used materials in the building sector today [14], to investigate the molecule's potential for corrosion on Fe(111). Hence, the main aim of the study is using a computational approach or method to look at the adsorption potentials of the acid complex carbamodithionic acid. Despite reports in the literature that Fe(110) crystal has a higher linear density ( $\lambda$ ) than Fe(111), the authors chose to test the molecule's potential on the Fe(111) surface.



**Scheme 1:** Carbamodithionic acid (CTA) structure

## Computational Methods

### Molecular Geometric Optimization

ChemDraw Ultra 7.0.3 CambridgeSoft was used to sketch the investigated compound of the investigated compound. The molecular structure was optimized to a stable configuration which changes the atoms' coordinates to a stationary point. In order to get the energy of the structure to a stationary point, or when the forces acting on the atoms are zero, the coordinates of the atoms are repeatedly modified during this process. The geometry corresponding to this structure is expected to be quite similar to the actual physical structure of the system when it is in equilibrium [6-8]. Using the DMol3 optimization tool of BIOVIA Materials Studio 8.0, the torsional and conformational energy of the molecules were lowered (Accelrys, Inc.). After importing the chemical into Materials Studio from Chemraw, restricted spin polarization was used as the basis for optimization. The optimization was performed using the restricted spin

polarization DNP+ foundation for DFT. The local density functional in the water solvent was selected to be B3LYP [1-3].

### Calculation of Energy Parameters

Dmol3 is a program that uses first principles calculations to determine the electronic characteristics of crystalline solid materials, surfaces, and clusters of molecules in order to find the optimal molecules' lowest energy [12]. The double numeric with polarization (DNP) basis set, the exchange component's functional methods B3LYP from the name Becke, and the correlation component's Lee, Yang, and Parr were used in the DFT computation. Equations (2) and (3), respectively, relate the energy of the border molecular orbital, the energy of the highest occupied molecular orbital ( $E_{HOMO}$ ), and the energy of the lowest unoccupied molecular orbital ( $E_{LUMO}$ ), in accordance with Koopman's theory [14-17].

$$IE = -EHOMO \quad (1)$$

$$EA = -ELUMO \quad (2)$$

According to Pearson, Equation (3) provides an approximate description of the value of global hardness ( $\eta$ ). Equation (4) depicts the global softness ( $S$ ) of the system, which is the opposite of the global hardness.

$$\eta = \frac{IE-EA}{2} \quad (3)$$

$$S = \frac{1}{\eta} \quad (4)$$

Equation (5) provides a connection for calculating the molecules' energy gap.

$$\Delta Eg = ELUMO - EHOMO \quad (5)$$

Equation (6) is used to determine the proportion of electrons that are transported from the inhibitor to the Fe-surface, or  $\Delta N$ . The molecules' half electron transfer is a measure of how well the inhibition process works, and it is dependent on both the electron transfer and the molecule's size.

$$\Delta N = \frac{\chi_{Fe} - \chi_{Inh.}}{2(\eta_{Fe} + \eta_{Inh.})} \quad (6)$$

When a molecule obtains a certain quantity of charge,  $\Delta N+$ , it may be described as follows using the basic charge transfer model for donation and return donation of charges:  $\Delta E+ = \mu+ \Delta N+ + 1/2(\Delta N+)^2$  and  $\Delta E- = \mu- \Delta N- + 1/2(\Delta N-)^2$  occurs when a molecule back-donates a certain amount of charge,  $\Delta N-2$ . The overall energy change will roughly equal the sum of the contributions, assuming that the charge back-donation is equal to the charge received [15-18].

$$\Delta E_t = \Delta E+ + \Delta E- \quad (7)$$

However, the most advantageous scenario is one in which the overall energy change ( $\Delta E$  back-donation) approaches zero in relation to  $\Delta N+$ , suggesting that:

$$\Delta E_{bd} = (\mu+ - \mu-)^2 / 4 \eta = \frac{-\eta}{4} \quad (8)$$

Equations (9) and (10) define the electron donating ( $\omega-$ ) and electron receiving ( $\omega+$ ) powers of the molecules, correspondingly [19].

$$\omega- \approx \frac{(3I+A)^2}{16(I-A)} \quad (9)$$

$$\omega+ \approx \frac{(I+3A)^2}{16(I-A)} \quad (10)$$

Where,

$\chi$  = Absolute electronegativity (eV)

$$\chi = \frac{I+A}{2} = \frac{-1}{2}(EHOMO - ELUMO) \quad (11)$$

With a theoretical electronegativity value of  $\chi_{Fe}=7.0\text{eV}$  and a global hardness of  $0\text{eV}$ , the metal and molecule were described as donating and acceptably by dual descriptor  $\Delta f(k)$  [2-5]. Equation (11) defines the second Fukui function or dual description as the difference between the nucleophilic and electrophilic Fukui functions. Site K favors an electrophilic attack when  $f_2(r)$  is less than zero, and a nucleophilic assault when  $f_2(r)$  is greater than zero. This suggests that  $f_2(r)$  functions as a selectivity index for assaults that are either electrophilic or nucleophilic [14,19-20].

$$f(k)+: \text{ (for nucleophilic attack) } = qk(N + 1) - qk(N) \quad (12)$$

$$f(k): \text{(for electrophilic attack)} = qk(N) - qk(N-1) \quad (13)$$

$$f(r) = f^+ - f^- = f^2 \quad \text{(Fukui function)} \quad (14)$$

### Molecular Dynamics Simulation

The surface of the metal Fe was split along the (1 1 1) Plane using COMPASS FORCEFIELD and Smart ALGORITHM in a simulation box of 17 x 12 x 28 with a periodic boundary condition and a fractional depth of 3.0. Before surface optimization, the lower layers' form was constrained to reduce the crystal's edge effects. The supercell 4 x 4 was signed to the crystals on the metal surface [1-4]. To quench the molecules on the surface, a fixed temperature of 350 K was applied to the system [21]. The temperature was set using the NVE ensemble, with a simulation time of 5 ps and a time step of 1 fs. The system was set up to quench on both surfaces every 250 steps in order to acquire the statistical values of the energy on the surfaces of Al and Fe. Utilizing forcite customized surface and molecular designs, various interactions were generated to calculate the binding energy between the inhibitors and the metal surfaces using the relation found in Equation (14) [22].

$$\text{Binding Energy} = E_{\text{total}} - (E_{\text{inhibitor}} + E_{\text{Fe surface}}) \quad (14)$$

## Results and Discussion

### Geometries of Carbamodithionic Acid (CTA) Molecule

The structure of the inhibitor molecule (CTA) is shown in Figure 1 to indicate the atoms present in the compound. The bond length, sometimes called the bond distance, is the average distance between two bonded atoms in a molecule [12]. The bond lengths of the molecules for the ideal geometry and structure at 353 K are shown in Armstrong (Å) in Figure 2. The structure of the molecule matched its lowest energy conformer provided the information used in this research. The examined CTA molecule had completely planar

optimized structure both before and after simulation, as shown by the optimized structure and bond angle values [15]. This suggests that the molecule will probably adsorb in a flat orientation on a metal surface, maximizing surface coverage [23-24]. The bond lengths in the molecule were compared between the simulated and un-stimulated versions to understand how molecular interaction with the Fe surface affects the strength of the bonds [12].

It is discovered that when the structural orientation of atoms in molecules shifts at 350K, the bond lengths of each atom in a molecule fluctuate. Comparing the bond length values in the structure, it was discovered that the bond lengths of C1-C4 rose dramatically from 1.644 nm to 3.769 nm, and the bond lengths of C1-S3 and C1-N2 increased in the same order. This implies that the molecule will effectively block the metal's experimental surface [17-18].

Planar (tend to 180° or 0°) bond angles are computed for the inhibitor, S4-C1-S3, S4-C1-N2, and N2-C1-S3. From the result, the compound is expected to exhibit strong p-orbital character in its SP<sup>2</sup> hybridization on the metal surface. This result is similar to Belghiti *et al.* geometric analysis on the [17].

### Frontier Molecular Orbitals of CTA

Using Dmol3, the optimal electron density, HOMO, and LUMO structures of the investigated CTA molecule were derived at the spin polarization DNP+ basis for the DFT B3LYP level of theory as presented in Figure 3.

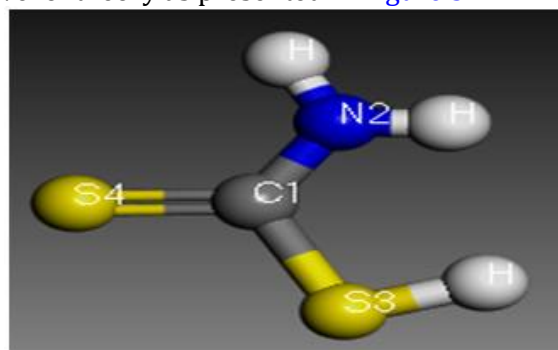
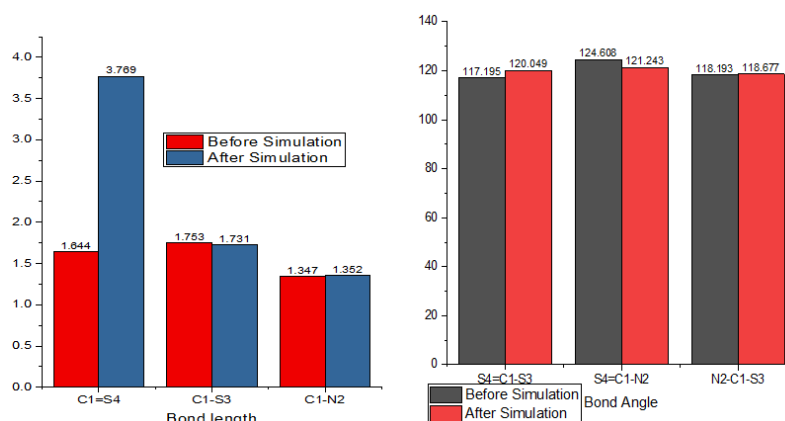
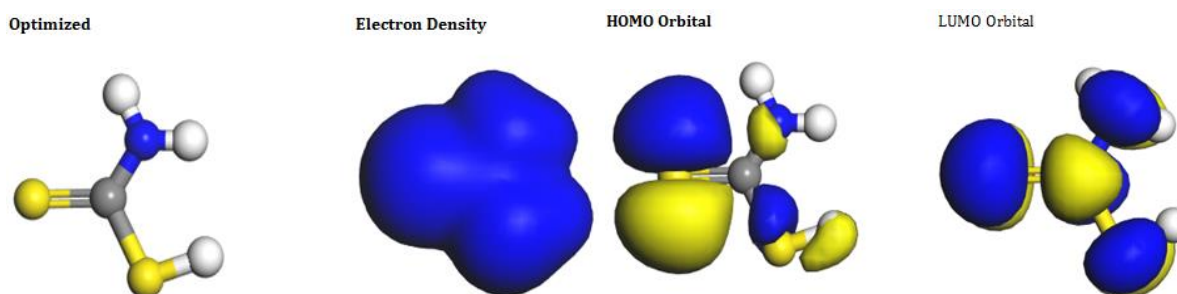


Figure 1: CDA molecular structure



**Figure 2:** Graphical Bond angles ( $\varphi^\circ$ ) and link length ( $\text{\AA}$ ) of the molecule



**Figure 3:** Optimized, electron density, HOMO and LUMO orbitals of the molecule CTA

Evidently, the molecule's HOMO and LUMO electron concentrations are dispersed through the atoms, but with focus on the hetero atoms of the molecule. This implies that, the potential active orbitals for donor-acceptor interactions are dispersed across the whole molecule, allowing it to donate electrons to the d-orbital of the Fe-surface and hence have more adsorptive qualities for the inhibition of the metal [10-15]. Although both surfaces reflect fundamentally -orbitals, the HOMOs displayed more -characters than the LUMOs.

### Frontier Energy of the Molecule

To examine the structure and behavior of corrosion inhibitors, quantum chemical approach is particularly important in the study of corrosion [1-7]. The Dmol3 module was used to calculate the quantum chemical parameters of the molecule which include, energy of the highest occupied molecular orbital ( $E_{\text{HOMO}}$ ), energy of the lowest unoccupied molecular orbital ( $E_{\text{LUMO}}$ ), energy gap ( $E$ ), electron affinity

( $A$ ), ionization potential ( $I$ ), global hardness ( $\eta$ ), global softness ( $\sigma$ ), fraction of electron transfer Fe ( $\Delta N$ ), electron donating powers ( $\omega^-$ ) eV, electron accepting powers ( $\omega^+$ ), and back donation ( $\Delta E_{\text{b-d}}$ ).

The interaction between the reacting species' lowest unoccupied molecular orbital (LUMO) and highest occupied molecular orbital (HOMO) is what causes an electron transition, according to the frontier molecular orbital theory (FMO) of chemical reactivity.  $E_{\text{HOMO}}$ , which measures how efficiently a molecule can deliver electrons to the empty d-orbital of a metal [8-11], is typically used to determine a molecule's capacity to donate electrons.  $E_{\text{LUMO}}$  is frequently linked to a molecule's capacity to absorb electrons from the d-orbital of the metal surface, leading to the formation of a new bond [22]. Since the appropriate acceptor molecule has a low energy and an empty molecular orbital, larger values of  $E_{\text{HOMO}}$  suggest a stronger probability for the molecule to transfer electron(s) to its orbit [12]. As a result, large

values of  $E_{\text{HOMO}}$  encourage adsorption, improving inhibitory effectiveness. The molecules can effectively deliver electron to a metal's unoccupied d-orbital based on the structure examined and shown in Figure 4 [18]. This number is consistent with the results of Nyijime *et al.* [20]. A molecule with a lower  $E_{\text{LUMO}}$  value finds it easier to capture electrons from a metal surface's empty d-orbital, which leads to the formation of a new bond and increases the amount of energy released when an electron is added to the molecule's geometry-optimized molecular structure with the lowest  $E_{\text{LUMO}}$  value [24]. A crucial instrument for assessing the stability of the molecule throughout a process is the value of  $E$  ( $E_{\text{LUMO}} - E_{\text{HOMO}}$ ). Higher values of  $E$  result in strong stability and low reactant reactivity, which negatively impacts the inhibitor molecule's capacity to stop the reaction [25]. Because less excitation energy is needed to remove an electron from the last occupied orbital, smaller values of  $\Delta E_g$  result in improved inhibition efficiency [10-15].

Figure 4 indicates that the molecule has the low energy gap at the geometry-optimized structure, which is identical to the outcome discovered by Umar and Ayuba [1]. Global softness is the inverse of global hardness, which in this study corresponds to the  $E_{\text{HOMO}}$  and  $E_{\text{LUMO}}$  magnitudes. The fraction of electron transfer calculates the proportion of electrons that move from one substance to another. Figure 4 demonstrates that only 3.6 ratio of electrons were moved from the inhibitor to the iron metal's metallic surface. According to Lukovits *et al.* as reported by Verma [30], the result suggests that the inhibitors' capacity to contribute electrons to the metal surface enhanced the metal's inhibitory efficiency [4-7,17]. The electron donating power ( $\omega^-$ ) and electron receiving power ( $\omega^+$ ) of the molecules were calculated. According to Chattaraj *et al.* as reported by Glossman-Mitnik, a system with a lower ( $\omega^-$ ) electron donating power value is better at giving electrons, whereas a system with a greater ( $\omega^+$ ) electron accepting power value is more capable of receiving charge [19-22]. The conclusion drawn from the molecule is not supported by the varying values of electron

affinity and ionization energy. To further illustrate the inhibitor molecule's interaction with the metal surface, the reverse donation  $\Delta E_{\text{b-d}}$  energy might be used. Nyijime *et al.* assert that an increased back-donation process would result from a positive global hardness and a negative energy of back donation ( $\Delta E_{\text{b-d}}$ ) value [24-25], this result in similar to the result obtained by Nyijime *et al.* [17]. The fact that all of the molecules' global hardness values in Figure 4 are positive indicates that when the inhibitor comes into contact with the iron surface, the molecule will transmit its charge to the iron metal with ease [16].

#### Active site

The Fukui indices were used to examine the active sites of the inhibitor interaction with the surface nucleophilic ( $f^+$ ) and electrophilic ( $f^-$ ) attacks. The nucleophilic and electrophilic attacks are controlled by the maximum  $f^+$  and  $f^-$ , the highest values of the Fukui functions, respectively [24-25]. The primary targets of a nucleophilic attack are the atoms with the highest value of  $f^+$ . In the same way, electrophilic attacks are preferred when Fukui function has a largest value [12]. Figure 5 displays the calculated condensed Fukui functions for the investigated inhibitor compound. The S (4) atom of each inhibitor molecule has a larger Mulliken(M) charge, which is where nucleophilic and electrophilic assaults on the molecules mostly take place [14-15]. The examined inhibitor molecule's second-order Fukui functions reveal that it is 85.71% nucleophilic, which makes it more efficient at halting the corrosion of iron metal surfaces [13]. The results go on to demonstrate that only S (4) atoms experience electrophilic assault, with a 14.29% percentage value. According Martínez-Araya, The dual descriptor allows one to obtain simultaneously the preferably sites for nucleophilic attacks when ( $f^2 > 0$ ) and the preferably sites for electrophilic attacks when ( $f^2 < 0$ ) over the system. The result obtained has I that, CTA is more of nucleophilic attack. This result is similar to the result obtained by Ayuba and Ameenullah [31]. Figure 6 displays the molecule CTA on the Fe(111) surface both side and front view.

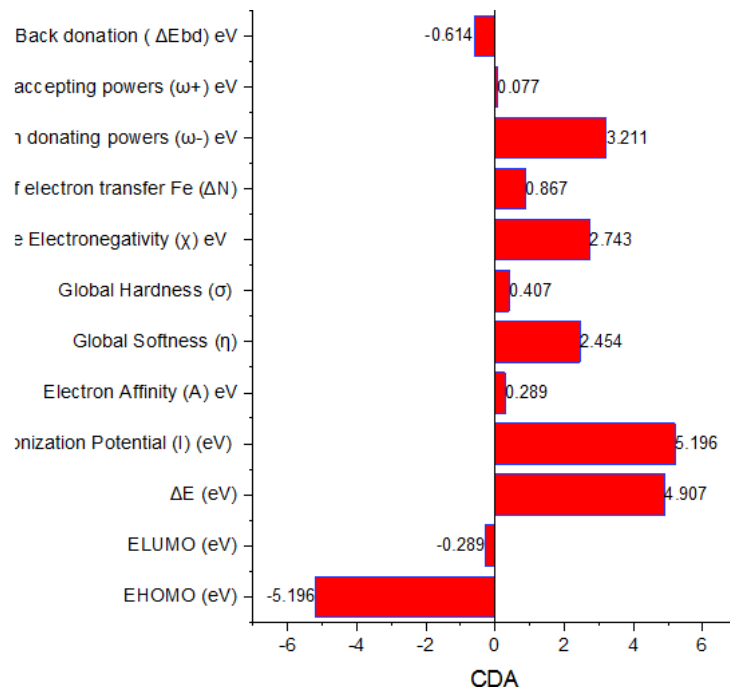


Figure 4: Graphical representation of calculated quantum chemical parameters for the molecule

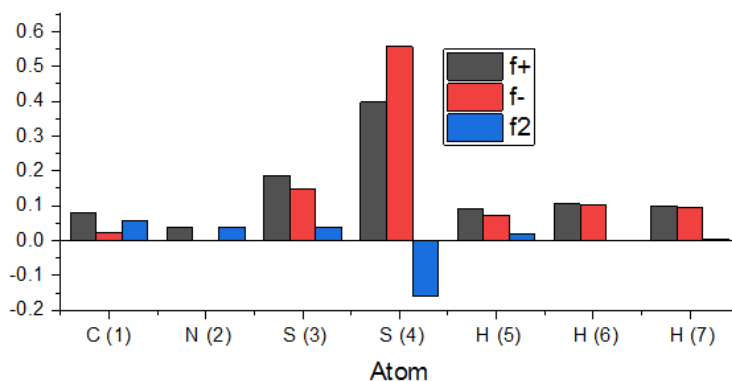
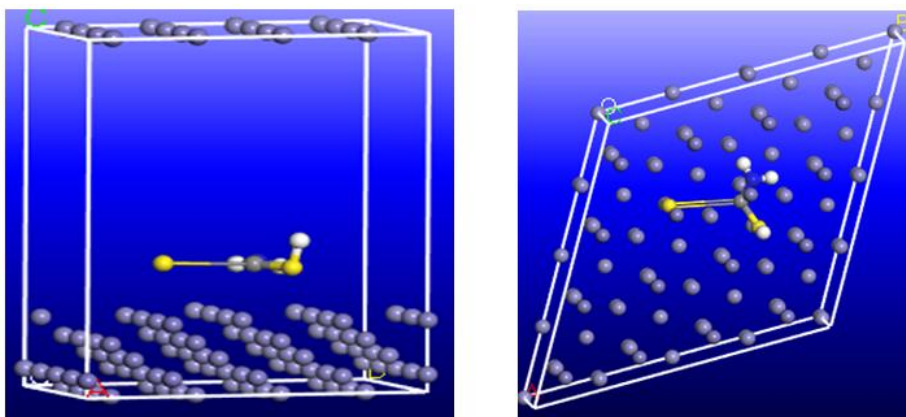


Figure 5: Active site of the molecule



Side view of the molecule on Fe (111)

Top view of molecule on Fe(111)

Figure 6: The studied molecule on top and side view as it was simulated on the surface of Fe (111) crystal

### Dynamic Simulation of Molecules

To evaluate the molecules adsorption on the metal surface, the molecular dynamic simulations were run, and Forcite quench was used to sample a wide range of low-energy configurations and locate the low-energy of the molecule [10]. The observed adsorption of inhibitor on mild steel was reproduced by modeling the interactions between the inhibitor and the Fe (111) crystal surface [20-21].

**Table 1:** Interaction energies of the CTA molecule on Fe(111) simulation

Properties (kJ.mol <sup>-1</sup> )	CTA
Energy of Fe (111)	0.000 ±0.0
Adsorption energy	-37.254±0.1
Binding energy	37.254±0.1

### Inhibition Mechanism

From Table 1, it was determined that the Cutoff distance between the molecules and the Fe(111) surface was 9.5 Å. This distance illustrates the ineffective orbital overlap and weak interaction between the orbitals, which can result in when the molecule is physically adsorbed onto the metal surface; metal-organic bonds are formed with very little energy [25]. From the Kinetic energy of the molecule on the surface the simulation indicated a slow motion of the molecule on the surface which give enough time for the molecule to interact with the surface [18]. The fact that the molecule's energy is 0 indicates that the iron's surface was entirely erased before the surface's energy was taken. Table 1 displays the amount of the molecule's interaction energy. The Table's low interaction energy record of -37.254 kJmol<sup>-1</sup> reveals a millimeter-scale adsorption on the Fe surface [2-4]. The higher the binding energy of the inhibition and the more negative adsorption energy of the system are, the more successfully the inhibitor will interact with the iron surface [10].

### Conclusion

Based on the values derived from the quantum chemical computation and Fukui indices, it is demonstrated that the active sites of the molecules are the S4=C1-S3 area on the ring, the heteroatoms (N and S), the pi-bond in the molecule, and the double-bonded carbon atoms in the molecule. The bond length analysis further demonstrates the efficiency of the hetero atoms with respect to the reactivity of the bonds they share with the carbon atom. The inhibitor's bond angles are planar (tend to be 180° or 0°), and it is anticipated that the compound will display SP<sup>2</sup> hybridization with a significant amount of p-orbital character on the metal. The quantum chemistry simulation also shows that neither the HOMO density nor the LUMO density, which can help with adsorption, are significantly increased by the thio functional group in the molecule or the pi-bond that is connected to the S4-C1 bond. The molecule can be used as a corrosion inhibitor on mild steel based on the given adsorption qualities since it has a reduced energy gap of 4.907 eV, a greater E<sub>HOMO</sub> of -5.196 eV, and a higher global softness of 2.454. In addition, the molecule's capacity for adsorption closely matches the binding energy at the temperature under consideration. Thus, to verify the molecule's inhibitory potential obtained from this research work using DFT and dynamic simulation, the author suggests experimental testing on the Carbamodithionic acid (CTA).

### Acknowledgements

We express our profound gratitude to the heads of the chemistry departments at Bayero University Kano (B.U.K.) and Joseph Saawuan Tarka University Makurdi (JOSTUM) for fostering an environment that enabled the study to be successful.

### Disclosure Statement

No potential conflict of interest was reported by the authors.

## Orcid

Ayuba A. Muhammad : 0000-0002-2295-8282

Nyijime A. Thomas : 0000-0001-9537-1987

Safiyya A. Minjibir : 0009-0006-4671-2670

Najib U. Shehu : 0000-0002-9145-9196

Fater Iorhuna : 0000-0002-1018-198X

## Reference

- [1]. H.A. AlMashhadani, K.A. Saleh, *Iraqi Journal of Science*, **2020**, 2751-2761. [[Crossref](#)], [[Google Scholar](#)], [[Publisher](#)]
- [2]. L. Afandiyeva, V. Abbasov, L. Aliyeva, S. Ahmadbayova, E. Azizbeyli, H.M. El-Lateef Ahmed, *Iranian Journal of Chemistry and Chemical Engineering*, **2018**, 37, 73-79. [[Crossref](#)], [[Google Scholar](#)], [[Publisher](#)]
- [3]. H. Jafari, F. Mohsenifar, K. Sayin, *Iranian Journal of Chemistry and Chemical Engineering (IJCCE)*, **2018**, 37, 85-103. [[Crossref](#)], [[Google Scholar](#)], [[Publisher](#)]
- [4]. S. Elmi, M.M. Foroughi, M. Dehdab, M. Shahidi-Zandi, *Iranian Journal of Chemistry and Chemical Engineering (IJCCE)*, **2019**, 38, 185-200. [[Crossref](#)], [[Google Scholar](#)], [[Publisher](#)]
- [5]. N. Noorollahy Bastam, H.R. Hafizi-Atabak, F. Atabaki, M. Radvar, S. Jahangiri, *Iranian Journal of Chemistry and Chemical Engineering*, **2020**, 39, 113-125. [[Crossref](#)], [[Google Scholar](#)], [[Publisher](#)]
- [6]. L.T. Popoola, T.A. Aderibigbe, M.A. Lala, *Iranian Journal of Chemistry and Chemical Engineering*, **2022**, 41, 482-492. [[Crossref](#)], [[Google Scholar](#)], [[Publisher](#)]
- [7]. R.M. Kubba, N.M. Al-Joborry, *Iraqi Journal of Science*, **2021**, 1396-1403. [[Crossref](#)], [[Google Scholar](#)], [[Publisher](#)]
- [8]. K.A.K. Al-Rudaini, K.A.S. Al-Saadie, *Iraqi Journal of Science*, **2021**, 363-372. [[Crossref](#)], [[Google Scholar](#)], [[Publisher](#)]
- [9]. M.A. Mohammed, R.M. Kubba, *Iraqi Journal of Science*, **2020**, 1861-1873. [[Crossref](#)], [[Google Scholar](#)], [[Publisher](#)]
- [10]. S. Mammeri, N. Chafai, H. Harkat, R. Kerkour, S. Chafaa, *Iranian Journal of Science and Technology, Transactions A: Science*, **2021**, 45, 1607-1619. [[Crossref](#)], [[Google Scholar](#)], [[Publisher](#)]
- [11]. T.V. Kumar, J. Makangara, C. Laxmikanth, N.S. Babu, *International Journal of Computational Theoretical Chemistry*, **2016**, 4, 1-6. [[Crossref](#)], [[Google Scholar](#)], [[Publisher](#)]
- [12]. T. Esan, O. Oyeneyin, A. Olanipekun, N. Ipinloju, *Advanced Journal of Chemistry-Section, A*, **2022**, 5, 263. [[Crossref](#)], [[Google Scholar](#)], [[Publisher](#)]
- [13]. R.M. Kubba, N.M. Al-Joborry, N.J. Al-Lami, *Iraqi Journal of Science*, **2020**, 2776-2796. [[Crossref](#)], [[Google Scholar](#)], [[Publisher](#)]
- [14]. Z. Yavari, M. Darijani, M. Dehdab, *Iranian Journal of Science and Technology, Transactions A: Science*, **2018**, 42, 1957-1967. [[Crossref](#)], [[Google Scholar](#)], [[Publisher](#)]
- [15]. N.M. Al-Joborry, R.M. Kubba, *Iraqi Journal of Science*, **2020**, 1842-1860. [[Crossref](#)], [[Google Scholar](#)], [[Publisher](#)]
- [16]. S. John, J. Joy, M. Prajila, A. Joseph, *Materials and corrosion*, **2011**, 62, 1031-1041. [[Crossref](#)], [[Google Scholar](#)], [[Publisher](#)]
- [17]. M. Belghiti, S. Echihi, A. Dafali, Y. Karzazi, M. Bakasse, H. Elalaoui-Elabdallaoui, L. Olanipekun, E. Ebenso, M. Tabyaoui, *Applied surface science*, **2019**, 491, 707-722. [[Crossref](#)], [[Google Scholar](#)], [[Publisher](#)]
- [18]. M.M. Kadhim, L.A.A. Juber, A.S. Al-Janabi, *Iraqi Journal of Science*, **2021**, 3323-3335. [[Crossref](#)], [[Google Scholar](#)], [[Publisher](#)]
- [19]. D. Glossman-Mitnik, *Procedia Computer Science*, **2013**, 18, 816-825. [[Crossref](#)], [[Google Scholar](#)], [[Publisher](#)]
- [20]. A. Nahlé, R. Salim, F. El Hajjaji, M. Aouad, M. Messali, E. Ech-Chihbi, B. Hammouti, M. Taleb, *RSC advances*, **2021**, 11, 4147-4162. [[Crossref](#)], [[Google Scholar](#)], [[Publisher](#)]
- [21]. N.O. Eddy, P.O. Ameh, N.B. Essien, *Journal of Taibah University for Science*, **2018**, 12, 545-556. [[Crossref](#)], [[Google Scholar](#)], [[Publisher](#)]
- [22]. L. Guo, M. Zhu, J. Chang, R. Thomas, R. Zhang, P. Wang, X. Zheng, Y. Lin, R. Marzouki, *International Journal of Electrochemical Science*, **2021**, 16, 211139. [[Crossref](#)], [[Google Scholar](#)], [[Publisher](#)]
- [23]. H. Lgaz, S. Masroor, M. Chafiq, M. Damej, A. Brahmia, R. Salghi, M. Benmessaoud, I.H. Ali, M.M. Alghamdi, A. Chaouiki, *Metals*, **2020**, 10, 357. [[Crossref](#)], [[Google Scholar](#)], [[Publisher](#)]
- [24]. F. Iorhuna, N.A. Thomas, S.M. Lawal, *Algerian Journal of Engineering and Technology*,

- 2023**, *8*, 43-51. [[Crossref](#)], [[Google Scholar](#)], [[Publisher](#)]
- [25]. G. Kılınççeker, M. Baş, F. Zarifi, K. Sayın, *Iranian Journal of Science and Technology, Transactions A: Science*, **2021**, *45*, 515-527. [[Crossref](#)], [[Google Scholar](#)], [[Publisher](#)]
- [26]. T. Nyijime, H. Chahul, A. Ayuba, F. Iorhuna, *Advanced Journal of Chemistry-Section A*, **2023**, *6*, 141. [[Crossref](#)], [[Google Scholar](#)], [[Publisher](#)]
- [27]. O. Oyeneyin, B. Obadawo, F. Ojo, D. Akerele, E. Akintemi, B. Ejelonu, N. Ipinloju, *Advanced Journal of Chemistry Section B*, **2020**, *2*, 197-208. [[Crossref](#)], [[Google Scholar](#)], [[Publisher](#)]
- [28]. F. Iorhuna, A.M. Ayuba, T.A. Nyijime, H. Muhammedjamiu, *Eurasian Journal of Science and Technology*, **2023**, *3*, 217-228. [[Crossref](#)], [[Google Scholar](#)], [[Publisher](#)]
- [29]. E.I. Edachea, H.A. Dawia, F.A. Ugbeb, *Journal of Applied Organometallic Chemistry*, **2023**, *3*, 224-244. [[Crossref](#)], [[Google Scholar](#)], [[Publisher](#)]
- [30]. D.K. Verma, *Advanced engineering testing*, **2018**, *87*. [[Crossref](#)], [[Google Scholar](#)], [[Publisher](#)]
- [31]. J.I. Martínez-Araya, *Journal of Mathematical Chemistry*, **2015**, *53*, 451-465. [[Crossref](#)], [[Google Scholar](#)], [[Publisher](#)]
- [32]. A. Muhammad Ayuba, A. Ameenullah, *Algerian Journal of Engineering and Technology*, **2020**, *3*, 028-037. [[Crossref](#)], [[Google Scholar](#)], [[Publisher](#)]

---

Copyright © 2023 by SPC ([Sami Publishing Company](#)) + is an open access article distributed under the Creative Commons Attribution License(CC BY) license (<https://creativecommons.org/licenses/by/4.0/>), which permits unrestricted use, distribution, and reproduction in any medium, provided the original work is properly cited.